Electrical and Spectroscopic Characterization of Molecular Junctions

James G. Kushmerick, David L. Allara, Thomas E. Mallouk, and Theresa S. Mayer

Abstract

The design of future molecular electronic devices requires a firm understanding of the conduction mechanisms that determine their electrical characteristics. Progress toward this goal has been hindered by complications in controlling the exact configuration and makeup of fabricated molecular junctions, thus limiting the availability of quantitative experimental data for developing cohesive theories to model and predict molecular transport. This article summarizes recent research aimed at developing well-controlled systems for comparing molecular conduction and vibrational spectra using crossed-wire and in-wire metal–molecule–metal junctions. Systematic variations in molecular structure and metal–molecule contacts show strong quantitative agreement in device properties, while spectroscopic data provide evidence that the properties are due to the molecular junction. Further investigations using these and other molecular junction test beds will provide the needed experimental data to advance fundamental understanding of molecular transport and facilitate future molecular electronics applications.

Keywords: *inelastic tunneling spectroscopy, molecular devices, molecular electronics, molecular wires, metal–molecule–metal junctions, self-assembled monolayers.*

Introduction

The field of molecular electronics is being driven by the potential to reduce the size of electronic, optical, and sensory devices to the scale of a single molecule. Innovations in synthetic chemistry have made it possible to tailor the electronic properties of molecules to serve as insulators and conductors as well as two- and three-terminal nonlinear devices.[1] These advances have sparked considerable activity in developing logic and memory architectures based on molecular devices that are scalable in terms of circuit density, power dissipation, and fabrication cost. Proposals range from long-term strategies for the self-assembly of complex logic elements from molecular wires and nonlinear devices[2] to nearer-term strategies that incorporate molecular monolayer junctions in logic and memory fabrics.[3] Ultimately, their success is predicated upon the ability to relate the terminal characteristics of single-molecule or monolayer devices to the physical phenomena affecting the underlying transport mechanisms.

Many test beds have been developed to characterize the electrical properties of molecular junctions and are the subject of several excellent reviews.[4] Briefly, measurements have been taken on single molecules using scanning probe contacts[5,6] and controllable break junctions.[7] Self-assembled monolayer (SAM) junctions have been characterized with top metal contacts formed using atomic force probes,[8] mercury drops,[9] low-temperature evaporation,[10] electroless deposition,[11] and crossed metal wires.[12,13]

These studies have provided experimental evidence for conduction through aromatic molecular wires and switching in nitroaromatic and rotaxane molecules as well as Coulomb blockade and Kondo effects in C_{60} and molecules incorporating transition-metal atoms.[5–13] These data and related modeling results have also shown that the terminal characteristics of molecular devices are not completely defined by the molecular structure, but are also strongly dependent on the environment in which the molecule resides (i.e., details of metal–contact interface and bonding; single-molecule versus SAM junctions, etc.).

Because the nature of the junction is strongly influenced by the molecule assembly conditions and the method used to form the top and bottom contacts, it is not surprising that data collected using different test beds often reveal qualitatively similar trends in behavior but quantitatively different device characteristics. These discrepancies must be addressed and understood through well-controlled independent studies that systematically vary the molecular structure and contacts. In addition, spectroscopic techniques should be developed and routinely employed to confirm that the measured transport properties are due to the molecular structure rather than artifacts of the device test bed.

In this article, we will describe initial progress toward these objectives by comparing the current–voltage (I–V) characteristics of two types of metal–SAM–metal structures—crossed-wire and in-wire junctions—produced using complementary fabrication procedures.

The crossed-wire junction is formed by bringing a micrometer-scale bare wire and a SAM-derivatized wire into contact in a crossing geometry. This test bed is well suited for investigating transport in molecular junctions because it minimizes the potential to introduce contaminants and monolayer damage, which is difficult to achieve in deposited top-contact junctions. Thus, it is a "clean" system that can serve as a reference standard.

In contrast, the in-wire structure incorporates SAM junctions within metallic nanowires prepared by electrochemical template replication. Here, molecules are assembled onto single-crystal nanowire tips, and top contacts are formed by room-temperature electroless seeding onto the SAM. In-wire devices are distinguished from most other test beds because they can be synthesized in large quantities (i.e., $\sim 10^{11}$ in each synthetic run) and have an aspect ratio appropriate to serving as building blocks for the bottom-up assembly of molecular electronic circuits.

We have investigated changes in conductance resulting from systematic variations in molecular structure[14,15] and metal–molecule contacts[14,16] for both test beds and find good agreement between the two.

In addition, we have applied inelastic electron tunneling spectroscopy (IETS)[17] to these junctions and have shown that *in situ* chemical characterization of metal–molecule–metal junctions is possible.

Experimental Considerations

We compared junctions formed using three molecules that are expected to have significantly different values of conductance: saturated alkyl chains of dodecane (C12), π-conjugated oligo(phenylene ethynylene) (OPE), and oligo(phenylene vinylene) (OPV) (see Chart 1). While relatively uninteresting for circuit applications, alkyl monolayers have become a standard for comparing the efficacy of different junction test beds, as experimental procedures have been established to form well-ordered SAMs on Au and other metal surfaces.[18] In addition, simple analytical models are available to adequately describe the tunneling mechanism that dominates transport through these molecules.[19] In contrast, junctions of π-conjugated molecular wires and their derivatives have considerably higher conductance (OPE and OPV) and nonlinear *I–V* (–NO_2 substituted OPE, NOPE) characteristics, which make them attractive for practical use.[1] However, the self-assembly procedures for forming monolayers of these molecular wires have only recently been studied, and models for predicting electron and hole transport are less well-developed. This section will describe recent progress in optimizing molecular wire self-assembly for junction devices and the procedures used to fabricate crossed-wire and in-wire molecular junctions.

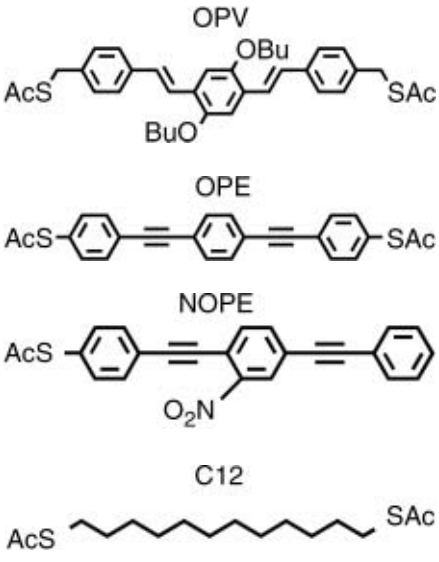

Chart 1. Structures of oligo(phenylene vinylene) (OPV), oligo(phenylene ethynylene) (OPE), –NO_2 substituted OPE (NOPE), and thioacetate-protected dodecane (C12) molecules used for self-assembly, junction conductance, and inelastic tunneling spectroscopy studies. Some results reported in this article use molecules with different end-group configurations (see text).

Self-Assembled Monolayers

One of the most important steps in fabricating molecular junctions is the chemical attachment of a single molecule or ensemble of molecules to at least one fixed electrode surface, typically through solution chemisorption. In cases where molecular ensembles are incorporated, the resulting film composition can vary from single-component to multicomponent. A common example of the latter is the preparation of monolayers in which active guest molecules are inserted into an "insulating" host-matrix SAM (e.g., hydrocarbon-type molecules).[20] There are two critical considerations for preparing reliable test-bed structures such as those described in this article: (1) the molecules must be chemically bonded in a uniform way to the fixed electrode, and (2) the SAMs must have physical and chemical integrity. Failure to provide good contact bonding can lead to low, irreproducible currents and instabilities, while missing molecules can cause shorts and dynamic degradation under bias. Surface contamination can lead to corrupted junctions with erratic or misleading electrical responses, and SAM impurity molecules can lead to ambiguities in interpreting *I–V* behavior.

Currently, most molecular devices involve –S– bonds to Au electrodes,[21] a useful system because of the large variety of molecules readily synthesized with a thiol end group (–SH) and the general chemical inertness of Au surfaces to troublesome side reactions such as corrosion or oxidation. Alternate Au contacts include isonitrile end groups (–NC),[22] with some limited work on –Se– attachment.[21,23] Varying the electrode material requires surfaces that can be kept bare during the molecular attachment process. The fairly inert noble metals Pt and Pd appear to be useful candidates.[16] The possibility of using diazonium chemistry to form highly stable molecular layers on bare Si surfaces by means of direct Si–C bonds also appears promising.[24]

For most test beds, it is nearly impossible to verify critical details of the chemical attachment and molecular configurations by conventional molecular-specific surface-science tools such as infrared spectroscopy (IRS), x-ray photoelectron spectroscopy (XPS), and scanning probes—atomic force microscopy (AFM) and scanning tunneling microscopy (STM). In general, one presumes that characterization done on large-area planar structures applies to small structures made under the same conditions. Currently, the only dependable way to characterize molecular structure in junctions is by direct IETS measurements of the junctions at low temperatures, as will be described.

An example of the issues that can arise in fabricating SAM junctions is given by recent work[25] on assembling thiol-terminated OPE and NOPE molecules. The –SH unit in these and similar aromatic thiols is somewhat unstable to air oxidation, so it is typically stabilized by conversion to a thioacetate –$SCOCH_3$ (or –SAc) group. Just prior to assembly, the thioacetate group is cleaved in acidic or basic solution, and then the bare Au surface is immersed into this solution to form a SAM. While this strategy works well for OPE, surprisingly, base cleavage of the NOPE SAM, the prevalent method in the recent literature, causes a side reaction that converts the –NO_2– to an amino (–NH_2) group. A combination of XPS and IRS characterization shows that a mixed SAM forms with as much as 30% –NH_2 component.[25] Clearly, structure/*I–V* correlations on junctions comprising these mixed SAMs would be ambiguous. In contrast, use of the pure thiol or acid cleavage results in well-organized, pure SAMs, as shown in Figure 1. Finally, it is noted that the best NOPE SAM preparations were done in a controlled, O_2-free atmosphere with degassed, high-purity solvents (e.g., tetrahydrofuran or ethanol) and that significant postdeposition cleaning was needed to remove ubiquitous, adventitious surface contaminants before good scanning probe images could be obtained.

Crossed-Wire Junctions

The crossed-wire junction avoids many of the limitations associated with deposited top contacts by eliminating the potential of metal atoms penetrating defects or reacting with the monolayer during junction fabrication. This makes the method well suited for these comparative transport studies. Figure 2a is a schematic representation of the crossed-wire test bed.[12] Two 10-μm-diameter metal wires, one derivatized with a SAM, are mounted into a custom-designed test stage such that the wires are in a crossed geometry with one wire perpendicular to the applied magnetic field. The junction separation is controlled by deflecting this wire with the Lorentz force generated from a small dc current flowing through the wire. This deflection current is slowly increased

to bring the wires together, forming a junction at the point contact. Different molecules, end groups, and metal wires can be incorporated into this test bed because of the relative simplicity with which junctions can be formed.

In-Wire Junctions

In contrast to the crossed-wire test bed, template-based nanofabrication methods are used to fabricate in-wire metal–molecule–metal junctions, as shown in Figure 2b.[11] In this process, bottom metal nanowire segments are electrodeposited into alumina or polycarbonate mesoporous membranes with a 35 nm nominal pore diameter. After metal deposition, molecules are self-assembled on all of the nanowire tips (10^{10}–10^{11} in each 1-cm^2-diameter template) using chemical assembly techniques. The conditions used to grow the bottom metal segments result in single-crystal nanowires of metals including Au and Pd.[26] The resulting high translational order of the metal at the nanowire tip surfaces will assist the formation of well-organized molecular superlattices in their junctions. We believe this leads to very low defect monolayers, thereby increasing junction yield. Top contacts are formed by growing Ag or Pd nanoparticles on top of the monolayer by chemical or electrochemical reduction of Ag or Pd metal ions adsorbed onto the free thiol end of the molecules.[14] The nanoparticles serve as a protective layer that minimizes shorting of the molecular junction and as a seed layer to initiate growth of the top nanowire segment at a potential low enough to prevent desorption of the SAM (e.g., less than –0.4 V). This synthesis method can be extended to junctions that include many different molecule end groups as well as bottom and top metal contacts.

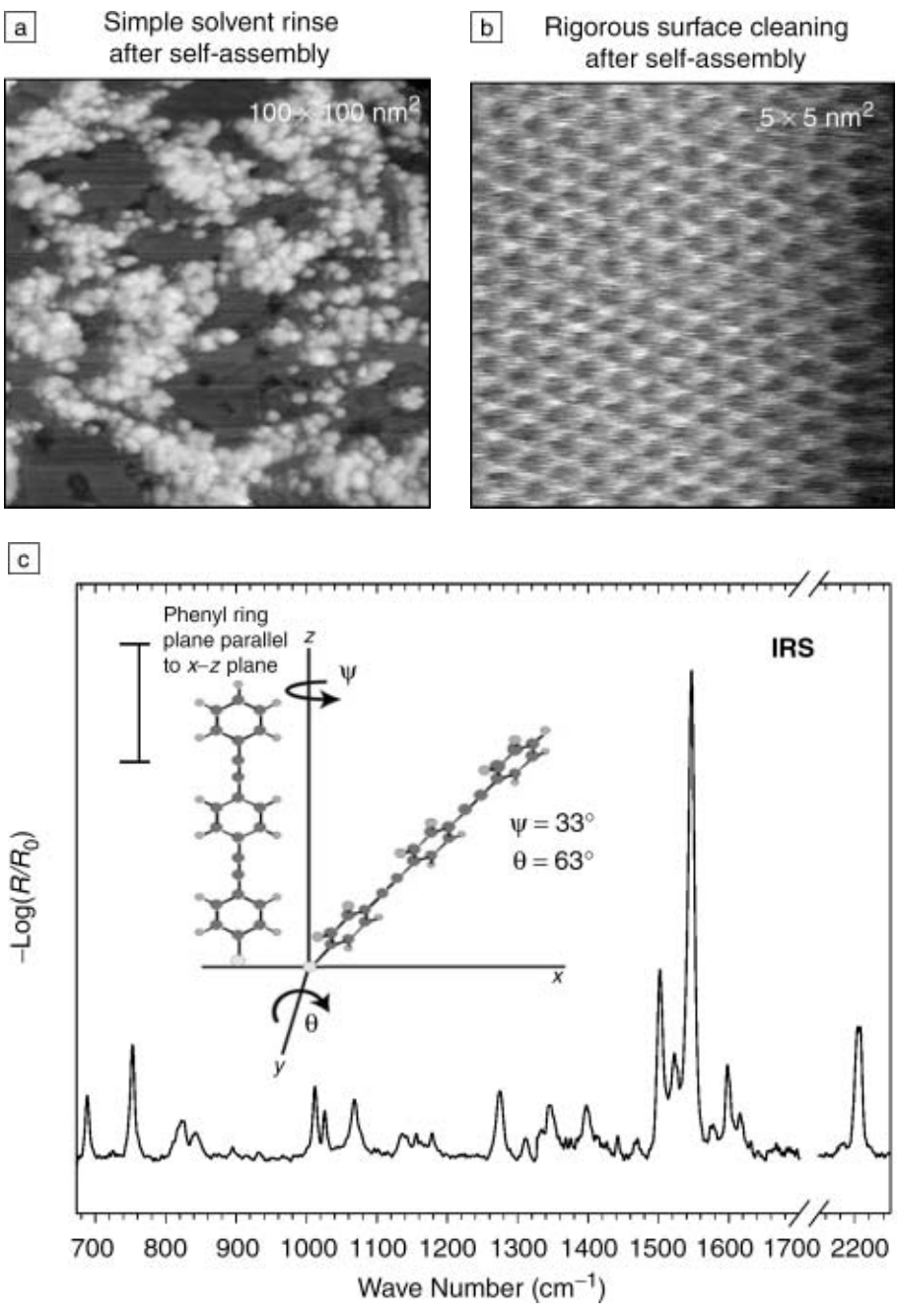

Figure 1. Infrared spectroscopy (IRS) and atomic force microscopy (AFM) data for a NOPE self-assembled monolayer (SAM) prepared from the pure thiol.[25] (a) Typical result, even from a careful preparation. (b) The molecular lattice that results if extreme care is taken to clean the SAM surface with various solvent treatments. (c) IRS spectrum resulting from a well-made sample. The spectral intensity is given by R/R_0, *where* R *is the power reflectivity of the sample and* R_0 *is the corresponding reflectivity of a bare Au surface that has been rigorously cleaned to remove adsorbed impurities. Obtaining a high-quality spectrum allows the determination of average tilt and twist angles for the molecules.*

Electrical testing is conducted on individual in-wire junctions after they are released from the template and aligned between pairs of large-area, lithographically defined Au electrodes by ac electric-field-assisted assembly.[27] The electrical connection between the nanowire and contact pad is formed by physical contact during assembly, eliminating all high-temperature postprocessing steps that could affect the molecular junction properties. Control experiments[14] made on solid Au and Pd nanowires show that the resistance associated with contact between the nanowire and electrodes is consistently less than 100 Ω, which is significantly lower than the resistance of the molecular junction. Thus, the conductance values reported in the following sections are those of the molecular junction.[14]

Molecular Conduction

A number of experiments have looked directly at the dependence of charge transport on molecular structure.[28–32] Figure 3 shows the room-temperature *I–V* characteristics measured for crossed-wire[15] and in-wire[14] junctions containing dithiolated C12, OPE, and OPV molecules.[14,15] Considering that both techniques form junctions with similar numbers of molecules, it is reassuring to see that measurements performed in both junction geometries show good agreement. As expected, there

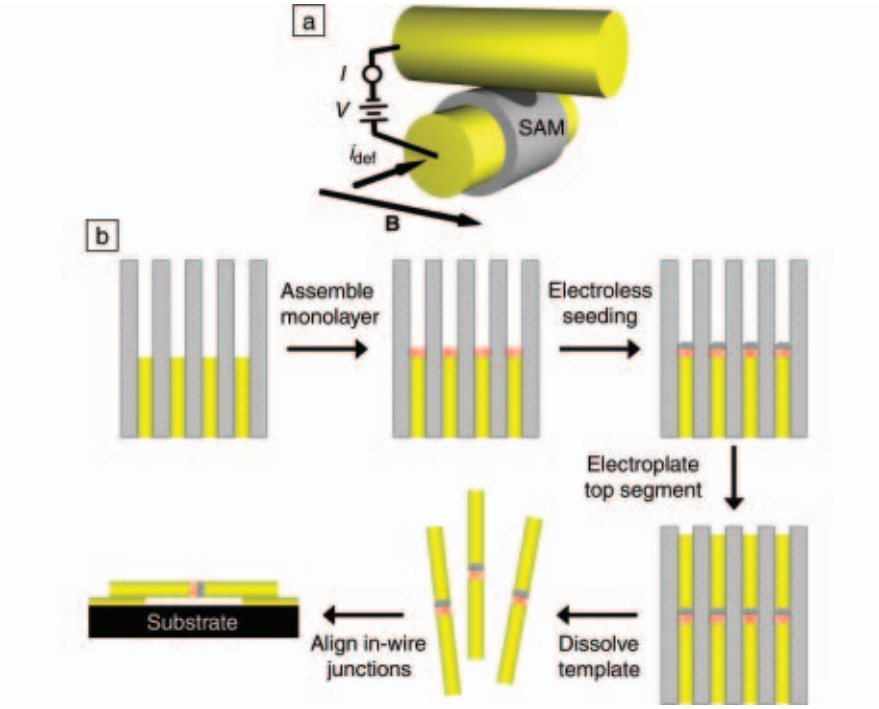

*Figure 2. Schematic representation of (a) a crossed-wire molecular junction, where i_{def} is the deflection current and **B** is the applied magnetic field. (b) In-wire junction fabrication steps. The final step of the in-wire sequence shows the nanowire contacting two large-area Au metal electrodes that are used for on-wafer probing of the molecular junction current–voltage (I–V) characteristics. Schematics are not to scale.*

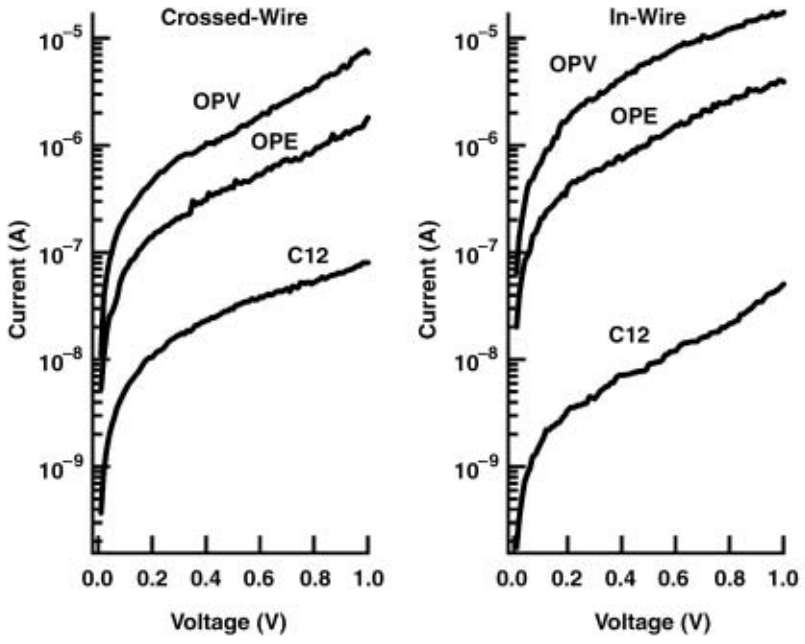

Figure 3. Room-temperature current–voltage (I–V) characteristics obtained for crossed-wire[15] and in-wire[14] junctions containing C12, OPE, and OPV self-assembled monolayers with Au-S bottom and Pd-S top contacts. The characteristics show that the conductance of OPV is greater than OPE, which in turn is greater than C12. The small differences in the characteristics measured using the two test beds are within the typical device-to-device variations observed on measurements of many junctions.

is a clear difference in the efficiency of charge transport across monolayers of electrically insulating alkane C12 and π-conjugated molecular wires of OPE and OPV. The difference in conductance between OPE and OPV is discussed next.

It has been argued previously that the higher coplanarity and thus better π-conjugation of OPV systems compared with OPE (in which the phenylene rings are freely rotating at room temperature) explain the more facile charge transport in OPV.[33,34] This is based on charge transport calculations that show that conductance is reduced when the phenyl rings of a conjugated system are rotated with respect to each other.[35,36] Notwithstanding the effect of coplanarity, there is a second important factor that affects a molecule's conductance, namely bond length alternation. If the molecules are considered to be one-dimensional crystals, the short (1.218 Å) ethynylene linkage (C≡C) in OPE disrupts the periodicity of the *p*-conjugated molecular backbone (1.41 ± 0.01 Å) more drastically than the vinylene linkage (C≡C) in OPV (1.352 Å, backbone = 1.41 ± 0.03 Å).

Studies of conducting polymers show that the size of the HOMO–LUMO gap (HOMO = highest occupied molecular orbit, LUMO = lowest unoccupied molecular orbit) is directly related to the extent of the bond length alternation.[37,38] The greater bond length alternation in OPE causes it to have a larger HOMO–LUMO gap than OPV (3.51 eV versus 3.12 eV). At low applied bias, transport is dominated by nonresonant tunneling inside the HOMO–LUMO gap. The difference in energy between the Au Fermi level and the closest molecular orbital (HOMO or LUMO) defines the tunneling barrier. The smaller HOMO–LUMO gap of OPV leads to a lower tunneling barrier and a higher conductance. In the language of solid-state physics, OPV can be thought of as having a smaller Peierls distortion than OPE, and thus it acts more like a one-dimensional metal.[39] Therefore, analyzing molecular conductance in terms of bond length alternation provides a new avenue for designing molecular wires with enhanced transport properties.

Metal–Molecule Contacts

The nature of the metal–molecule contact is controlled by the choice of chemical end group that connects the molecule to the electrode and the electrode metal. While Au–S contacts are the *de facto* standard, experimental and theoretical studies have shown that a significant increase in conductivity can be achieved by switching to Au–Se contacts.[40] Several groups have also reported that it is possible to form rec-

tifiers from molecular junctions that have asymmetric metal–molecule contacts—specifically, a strong Au–S bond at one interface and a weak nonbonding interaction at the other.[12,41] The electrode metal affects both the physical and electronic coupling, since the work function and metal–molecule bonding are both modified. Measurements of charge transport across alkyl monolayers suggest a correlation between a metal's work function and the contact resistance (i.e., junction resistance extrapolated to zero chain length).[42] Metals with higher work functions exhibited lower contact resistances, which was attributed to better hole injection due to enhanced coupling to the HOMO. Recent theoretical calculations on a π-conjugated molecular wire suggest that S-Pd is one of the best end-group/metal combinations, while the S-Au and S-Ag combinations are two of the worst.[36]

We fabricated molecular junctions with both mixed-metal electrodes (Au-OPE-Pd) and symmetric metal electrodes (Pd-OPE-Pd).[14,16] The transport properties of a crossed-wire junction formed from a monolayer of OPE between a Au and Pd wire is shown in Figure 4a. There is a small but distinct asymmetry in the *I–V* characteristics with 1.5 times more current at –1 V than at +1 V. In contrast, the *I–V* characteristics of a Au-OPE-Au junction (not shown) are completely symmetric. The measured *I–V* characteristics reflect the fact that the Pd-S interface exhibits a smaller barrier for charge injection than the Au–S interface. In fact, calculations have predicted that the Pd-S interface is nearly a barrierless contact.[36] Thus, the Au-S interface and transport through the molecule limit the overall conductance of the junction. The difference in injection barrier is even more apparent for in-wire junctions of the form Au-OPE-Ag and Pd-OPE-Pd (Figure 4b). The device that has Pd-S interfaces is nearly an order of magnitude more conductive than the device with Au-S and Ag-S contacts. These experiments demonstrate the important role that metal–molecule contacts play in determining the conductance of molecular devices. More extensive studies on a range of metal electrodes and end-group combinations are needed to optimize the conductance properties of molecular junctions.

In Situ Spectroscopy

One of the major difficulties in understanding and characterizing the function of molecules in molecular devices is the inability to use conventional spectroscopic methods to probe inside the metal–molecule–metal junction. Thus, there is often uncertainty as to whether the electronic response measured is an intrinsic property of the molecule or a defect/contaminant in the junction. Inelastic electron tunneling spectroscopy[43,44] is unique in its ability to directly measure the vibrational spectrum of molecular junctions, and as such, it provides an *in situ* probe to characterize and identify the molecular species under study by its vibrational "fingerprint." IET spectra are obtained by measuring the second derivative of the tunneling current with respect to the applied bias voltage (d^2I/dV^2). Peaks in d^2I/dV^2 versus V correspond to molecular vibrations. The one experimental requirement is that due to thermal broadening of the electron distribution about the Fermi level, IETS must be performed at cryogenic temperatures in order to have sufficient energy resolution to resolve the vibrational features.

Figure 5 is the IET spectrum of a crossed-wire junction formed from a monolayer of OPE.[17] From comparison to reflectance IR spectra of OPE monolayers[20] and calculations based on density functional theory, we tentatively assign the following vibrational features. The three prominent peaks at 138 mV, 196 mV, and 274 mV are assigned to the ν(18a) and ν(8a) ring modes and the C≡C stretch, respectively. The two ring vibrations are concerted C–C stretching and C–H bending modes of the three phenylene rings. There is also the suggestion of a C–H in-plane bending mode (57 mV). While the ν(18a) and ν(8a) ring modes are IR active and are prominent components of reflectance IR measurements of OPE monolayers, the C≡C stretch mode is primarily a Raman mode and appears vanishingly small in IR measurements.[25] The strong intensity of this Raman active mode in our IET spectrum demonstrates that both IR and Raman active modes are observed in IETS. Although IETS does not discriminate between IR and Raman active vibrational modes, there is still an orientation selection rule for the spectroscopy. The observed molecular vibrations all have a strong transition component perpendicular to the electrode surface. Given the junction geometry, the observed vibrations can be thought of as longitudinal modes of the metal–molecule–metal junction. Tunnel-

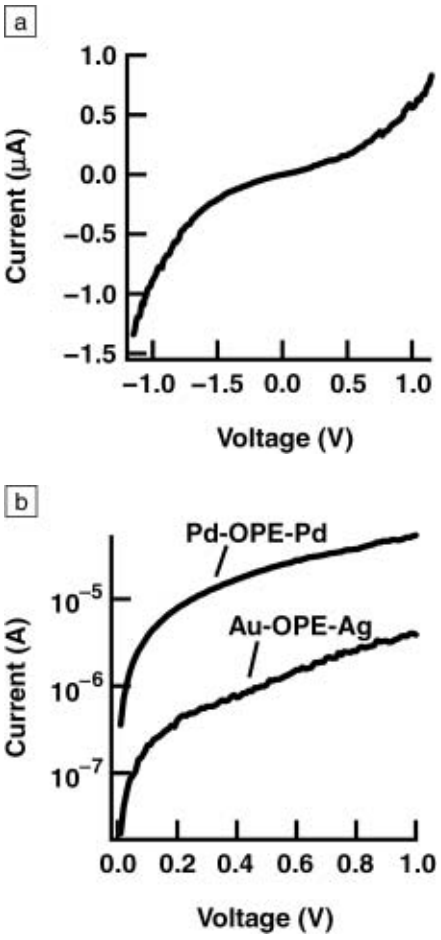

Figure 4. (a) Current–voltage (I–V) characteristics of a Pd-OPE-Au crossed-wire junction.[16] The higher conductivity of the negative branch of the I–V trace corresponds to hole injection at the Pd-S interface. (b) I–V characteristics of Pd-OPE-Pd and Au-OPE-Ag in-wire devices.[14] The current is increased by approximately one order of magnitude when Pd-S contacts are used in place of Au-S or Ag-S.

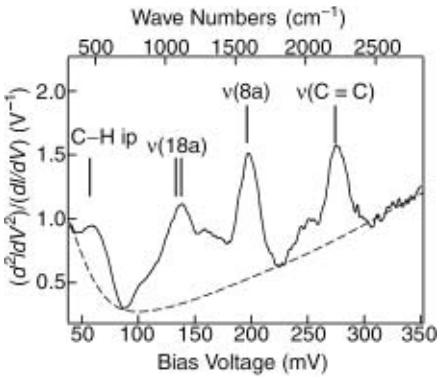

Figure 5. Inelastic electron tunneling (ITE) spectrum of an OPE crossed-wire junction measured at 4 K. The dashed line is a simple polynomial background and is presented as a guide to the eye. Although not shown, similar IET spectra have also been measured using in-wire junctions. C–H ip at 57 mV is a C–H in-plane bending mode, ν(18a) and ν(8a) are phenyl ring vibrations, and ν(C≡C) is the acetylene triple-bond stretching mode.

ing charge carriers couple strongly to dipole or polarizability changes of the molecules along their direction of travel. Such a longitudinal propensity rule for metal–molecule–metal junctions is supported by the recent theoretical analysis of Troisi, Ratner, and Nitzan.[45] The ability to determine the vibronic coupling associated with charge transport will provide important insight into the issue of local heating in molecular junctions.[46,47]

Summary and Future Directions

In this article, we presented experimental results from crossed-wire and in-wire test beds that show that conductance in molecular junctions is strongly dependent on both molecular structure and metal–molecule contacts. As predicted by theory, we observed large differences in charge transport through alkane C12 and π-conjugated OPE and OPV molecular junctions. The higher conductance of OPV as compared with OPE can be explained by its higher coplanarity and smaller bond length alternation (i.e., smaller HOMO–LUMO gap). Variations in metal/end-group contacts gave rise to changes in the symmetry of the *I–V* characteristics and conductance of the junctions. Asymmetric *I–V* behaviors were only noted on mixed-metal electrodes such as Au-Pd, which result in different barriers to charge injection for opposite bias polarities. The symmetric Pd-Pd junctions had the highest conductance of the metal/end-group combinations tested, which is expected from calculations that suggest the Pd-S interface produces one of the lowest –S barrier contacts. Agreement in the crossed-wire and in-wire junction characteristics indicate that robust molecule devices can be made using significantly different fabrication schemes if care is taken to control monolayer assembly and top metal deposition conditions.

We have also shown that inelastic tunneling spectroscopy can be applied directly to as-fabricated molecular junctions to determine the chemical identity of molecular species that contribute to conduction. IET spectra of crossed-wire OPE junctions contained three prominent peaks that correspond to the IR-active ν(18a), ν(8a) ring modes, and a Raman-active C≡C stretch mode of the OPE molecule. These data provide strong evidence that the measured junction properties are indeed due to the molecular structure, rather than being an artifact of the test bed. In addition, these measurements will facilitate an improved understanding of local heating in molecular junctions.

Further research using these and other test beds will continue to address molecular structure and contact effects as well as enable more thorough studies of mechanisms responsible for molecular switching, a requirement for applications involving molecular devices.[6,9,13] It is also expected that future temperature-dependent transport measurements will assist in elucidating the role of collective versus single-molecule effects in molecular junction conductance.[48]

Acknowledgments

The authors gratefully acknowledge our many graduate students, postdoctoral research associates, and colleagues who contributed to the research discussed in this article, especially S.K. Pollack, J. Naciri, and M.H. Moore (Naval Research Laboratory) for molecular synthesis, and L. Cai and J. Mbindyo (the Pennsylvania State University) for in-wire fabrication and measurement. The research discussed in this article was supported by DARPA/ONR under contracts ONR-N00014-98-1-0846 (PSU) and ONR-N00014-01-1-0657 (PSU), by DARPA (NRL), and by the NSF MRSEC Center for Nanoscale Science grant DMR-0213623 (PSU).

References

1. For example, see J.M. Tour, *Molecular Electronics* (World Scientific, River Edge, NJ, 2003).
2. For example, see J.C. Ellenbogen and J. C. Love, *Proc. IEEE* **88** (2000) p. 386.
3. For example, see S.C. Goldstein and M. Budiu, in *Proc. 28th Annu. Int. Symp. on Computer Architecture* (ACM Press, New York, 2001) p. 178.
4. For example, see B.A. Mantooth and P.S. Weiss, *Proc. IEEE* **91** (2003) p. 1785.
5. For example, see R.P. Andres, T. Bein, M. Dorogi, S. Feng, J.I. Henderson, C.P. Kubiak, W. Mahoney, R.G. Osifchin, and R. Reifenberger, *Science* **272** (1996) p. 1323.
6. For example, see Z.J. Donhauser, B.A. Mantooth, K.F. Kelly, L.A. Bumm, J.D. Monnell, J.J. Stapleton, D.W. Price, A.M. Rawlett, D.L. Allara, J.M. Tour, and P.S. Weiss, *Science* **292** (2001) p. 2303.
7. For example, see M.A. Reed, C. Zhou, C.J. Muller, T.P. Burgin, J.M. Tour, *Science* **278** (1997) p. 252; J. Reichert, R. Ochs, D. Beckmann, H.B. Weber, M. Mayor, and H.V. Löhneysen, *Phys. Rev. Lett.* **88** 176804 (2002); H. Park, J. Park, A.K.L. Lim, E.H. Anderson, P.A. Alivisatos, and P.L. McEuen, *Nature* **407** (2000) p. 57; J. Park, A.N. Pasupathy, J.I. Goldsmith, C. Chang, Y. Yaish, J.R. Petta, M. Rinkoski, J.P. Sethna, H.D. Abruna, P.L. McEuen, and D.C. Ralph, *Nature* **417** (2002) p. 722; W. Liang, M.P. Shores, M. Bockrath, J.R. Long, and H. Park, *Nature* **417** (2002) p. 725.
8. For example, see D.J. Wold and C.D. Frisbie, *J. Am. Chem. Soc.* **123** (2001) p. 5549; X.D. Cui, A. Primak, X. Zarate, J. Tomfohr, O.F. Sankey, A.L. Moore, T.A. Moore, D. Gust, G. Harris, and S.M. Lindsay, *Science* **294** (2001) p. 571.
9. For example, see R. Haag, M.A. Rampi, R.E. Holmlin, and G.M. Whitesides, *J. Am. Chem. Soc.* **121** (1999) p. 7895; J.D. Le, Y. He, T.R. Hoye, C.C. Mead, and R.A. Kiehl, *Appl. Phys. Lett*. **83** (2003) p. 5518.
10. For example, see J. Chen, M.A. Reed, A.M. Rawlett, and J.M. Tour, *Science* **286** (1999) p. 1550; M.A. Reed, J. Chen, A.M. Rawlett, D.W. Price, and J.M. Tour, *Appl. Phys. Lett*. **78** (2001) p. 3735.
11. For example, see J.K.N. Mbindyo, T.E. Mallouk, J.B. Mattzela, I. Kratochvilova, B. Razavi, T.N. Jackson, and T.S. Mayer, *J. Am. Chem. Soc.* **124** (2002) p. 4020.
12. For example, see J.G. Kushmerick, D.B. Holt, J.C. Yang, J. Naciri, M.H. Moore, and R. Shashidhar, *Phys. Rev. Lett.* **89** 086802 (2002).
13. For example, see C.P. Collier, E.W. Wong, M. Belohradsky, F.M. Raymo, J.F. Stoddart, P.J. Kuekes, R.S. Williams, and J.R. Heath, *Science* **285** (1999) p. 391.
14. L.T. Cai, H. Skulason, J.G. Kushmerick, S.K. Pollack, J. Naciri, R. Shashidhar, D.A. Allara, T.E. Mallouk, and T.S. Mayer, *J. Phys. Chem. B* **108** (2004) p. 2827.
15. J.G. Kushmerick, D.B. Holt, S.K. Pollack, M.A. Ratner, J.C. Yang, T.L. Schull, J. Naciri, M.H. Moore, and R. Shashidhar, *J. Am. Chem. Soc.* **124** (2002) p. 10654.
16. J.G. Kushmerick, S.K. Pollack, J.C. Yang, J. Naciri, D.B. Holt, M.A. Ratner, and R. Shashidhar, *Ann. N.Y. Acad. Sci.* **1006** (2003) p. 277.
17. J.G. Kushmerick, J. Lazorcik, C.H. Patterson, R. Shashidhar, D.S. Seferos, and G.C. Bazan, *Nano Lett.* **4** (2004) p. 639.
18. A. Ulman, *Chem. Rev.* **96 (**1996) p.1533; G.E. Poirier, *Chem. Rev.* **97** (1997) p. 1117.
19. L.A. Bumm, J.J. Arnold, T.D. Dunbar, D.L. Allara, and P.S. Weiss, *J.Phys.Chem. B.* **83** (1999) p.8122.
20. For example, see D.L. Allara, T.D. Dunbar, P.S. Weiss, L.A. Bumm, M.T. Cygan, J.M.Tour, T.P. Burgin, and L. Jones II, *Ann. N.Y. Acad. Sci.* **852** (1998) p. 349; M.T. Cygan, T.D. Dunbar, J.J. Arnold, L.A. Bumm, N.F. Shedlock, T.P. Burgin, L. Jones II, D.L. Allara, J.M. Tour, and P.S. Weiss, *J. Am. Chem. Soc.* **120** (1998) p. 2721.
21. R.G. Nuzzo and D.L. Allara, *J. Am. Chem. Soc.* **105** (1983) p. 4481.
22. J.G. Kushmerick, J. Naciri, J.C. Yang, and R. Shashidhar, *Nano Lett.* **3** (2003) p. 897.
23. J.D. Monnell, J.J. Stapleton, J.M. Tour, D.L. Allara, and P.S. Weiss, *J. Phys. Chem. B* (2004) in press.
24. M.P. Stewart, F. Maya, D.V. Kosynkin, S.M. Dirk, J.J. Stapleton, C.M. McGuiness, D. Allara, and J.M. Tour, *J. Am. Chem. Soc* **126** (2004) p. 370.
25. J.J. Stapleton, P. Harder, T.A. Daniel, M. Reinard, H. Skulason, Y. Yao, D.W. Price, J.M. Tour, and D.L. Allara, *Langmuir* **19** (2003) p. 8245.
26. M.L. Tian, J.U. Wang, J. Kurtz, T.E. Mallouk, and M.H.W. Chan, *Nano Lett.* **3** (2003) p. 919.
27. P.A. Smith, C.D. Nordquist, T.N. Jackson, T.S. Mayer, B.R. Martin, J.K.N. Mbindyo, and T.E. Mallouk, *Appl. Phys. Lett*. **77** (2000) p. 1399.
28. L.A. Bumm, J.J. Arnold, M.T. Cygan, T.D. Dunbar, T.P. Burgin, L. Jones II, D.L. Allara, J.M. Tour, and P.S. Weiss, *Science* **271** (1996) p. 1705.
29. M.T. Cygan, T.D. Dunbar, J.J. Arnold, L.A. Bumm, N.F. Shedlock, T.P. Burgin, L. Jones II, D.L. Allara, J.M. Tour, and P.S. Weiss, *J. Am. Chem. Soc.* **120** (1998) p. 2721.

30. D.J. Wold, R. Haag, M.A. Rampi, and C.D. Frisbie, *J. Phys. Chem. B* **106** (2002) p. 2813.
31. R.E. Holmlin, R. Haag, M.L. Chabinyc, R.F. Ismagilov, A.E. Cohen, A. Terfort, M.A. Rampi, and G.M. Whitesides, *J. Am. Chem. Soc.* **123** (2001) p. 5075.
32. A.S. Blum, J.C. Yang, R. Shashidhar, and B. Ratna, *Appl. Phys. Lett.* **82** (2003) p. 3322.
33. S.B. Sachs, S.P. Dudek, R.P. Hsung, L.R. Sita, J.F. Smalley, M.D. Newton, S.W. Feldberg, and C.E.D. Chidsey, *J. Am. Chem. Soc.* **119** (1997) p. 10563.
34. S. Creager, C.J. Yu, C. Bamdad, S. O'Connor, T. MacLean, E. Lam, Y. Chong, G.T. Olsen, J. Luo, M. Gozin, and J.F. Kayyem, *J. Am. Chem. Soc.* **121** (1999) p. 1059.
35. M.P. Samanta, W. Tian, S. Datta, J.I. Henderson, and C.P. Kubiak, *Phys. Rev. B* **53** (1996) p. R7626.
36. J.M. Seminario and P.A. Derosa, *J. Am. Chem. Soc.* **123** (2001) p. 12418.
37. A.J. Heeger, *J. Phys. Chem. B* **105** (2001) p. 8475.
38. R. Farchioni and G. Grosso, eds., *Organic Electronic Materials: Conjugated Polymers and Low Molecular Weight Organic Solids*, Vol. 41 (Springer, New York, 2001).
39. R.E. Peierls, *Quantum Theory of Solids* (Oxford University Press, London, 1955).
40. L. Patrone, S. Palacin, J. Charlier, F. Armand, J.-P. Bourgoin, H. Tang, and S. Gauthier, *Phys. Rev. Lett.* **91** 096802 (2003); and S.N. Yaliraki, M. Kemp, and M.A. Ratner, *J. Am. Chem. Soc.* **121** (1999) p. 342.
41. C. Zhou, M.R. Deshpande, M.A. Reed, L. Jones II, and J.M. Tour, *Appl. Phys. Lett.* **71** (1997) p. 611; A.-A. Dhirani, P.-H. Lin, P. Guyot-Sionnest, R.W. Zehner, and L.R. Sita, *J. Chem. Phys.* **106** (1997) p. 5249; J. Taylor, M. Brandbyge, and K. Stokbro, *Phys. Rev. Lett.* **89** (2002) p. 138301.
42. J.M. Beebe, V.B. Engelkes, L.L. Miller, and C.D. Frisbie, *J. Am. Chem. Soc.* **124** (2002) p. 11268.
43. R.C. Jaklevic and J. Lambe, *Phys. Rev. Lett.* **17** (1966) p. 1139.
44. B.C. Stipe, M.A. Rezaei, and W. Ho, *Science* **280** (1998) p. 1732.
45. A. Troisi, M.A. Ratner, and A. Nitzan, *J. Chem. Phys.* **118** (2003) p. 6072.
46. D. Segal and A. Nitzan, *J. Chem. Phys.* **117** (2002) p. 3915.
47. Y.-C. Chen, M. Zwolak, and M. Di Ventra, *Nano Lett.* **3** (2003) p. 1691.
48. Y. Selzer, M.A. Cabassi, T.S. Mayer, and D.L. Allara, *J. Am. Chem. Soc., Chem. Commun.* **126** (2004) p. 4052. □